ChemComm

Accepted Manuscript

This article can be cited before page numbers have been issued, to do this please use: X. Tian, Y. Zhu, M. Zhang, L. Luo, J. Wu, H. zhou, L. Guan, G. Battaglia and Y. Tian, *Chem. Commun.*, 2017, DOI: 10.1039/C6CC09470H.

ROYAL SOCIETY OF CHEMISTRY

rsc.li/chemcomm

Journal Name

View Article Online
DOI: 10.1039/C6CC09470H

COMMUNICATION

Localization Matters: A Nuclear Targeting Two-Photon Absorption Iridium Complex Induced Intracellular Immigration and Dual-damage in Photon Dynamic Therapy

Received 00th January 20xx,
Accepted 00th January 20xx

DOI: 10.1039/x0xx00000x
www.rsc.org/

Xiaohe Tian [ab‡], Yingzhong Zhu [b‡], Mingzhu Zhang [ab], Lei Luo [c], Jieying Wu [b], Hongping Zhou [b], Lijuan Guan [de], Giuseppe Battaglia [de], Yupeng Tian [bf*]*

Dedicated to Professor Yupeng Tian for celebration of his 60th birthday.

We present a two-photon (2P, 800nm) PDT cyclometalated Iridium (III) complex (Ir-Es) that targets intracellular nucleus, it is capable of imigrating sequentially from nucleus to mitochondria and inducing dual-damage under light exposure. It is suggest that with minor modification of complexes terminal moieties, their final intracellular destinations and PDT efficiency can significantly be impacted.

Photodynamic therapy (PDT) has drawn increasing attention over the past decades and has been successfully applied in treatment of certain types of cancer.[1] PDT is considered as a non-invasive treatment and relies on the use of combination of a photosensitizer (PS), light, and oxygen.[2] Generally, an ideal PS should present non-toxicity in absence of light. When excited under the selected laser，it reacts with the molecular oxygen ($^3O_2$) at ground state, consequently, generating $^1O_2$ and other reactive oxygen species (ROS),[3] which are considered as the primary toxic species at subcellular organelles or vasculature damage.[4] Although several PDT agents are clinically available, weak photostability, poor water solubility, high energy/shallow tissue penetration laser (excited from 400 to 700 nm) and excessed oxygen consuming still prevent their development.[5] Moreover, previous PDT agents including functionalized nano-particles are restricted to damage in one subcellular organelle (e.g. mitochondria and endoplasmic reticulum),[6] whereas nuclear or multi-organelle specific PSs are rarely existed. To tackle these barriers, two-photon (2P) PDT agents have been proposed to alter current PSs.[6a, 7] Compared with traditional PDT agents, 2P-PDT agents apply low energy near-infrared laser as light source, which displays significant benefits including less photobleaching of PSs and deeper tissue penetration.[8] Luminescent cyclometalated Iridium (III) complexes with two-photon absorption (2PA) behaviors have been widely investigated, particularly for their bio-application,[9] their utilization on PDT induced cell death was also well discussed.[10] Their main merits can be concluded as follows: (i) High photostability allows continuous irradiation and real-time monitoring of intracellular trafficking. (ii) Long-lived triplet states result in long lifetime and provide possible reaction with oxygen to generate ROS. (iii) Large Stokes Shift can minimize the possible self-quenching effect even in high concentration. (iv) Compatibility with two-photon excitation achieves deeper tissue-penetration and excellent resolution.[11]

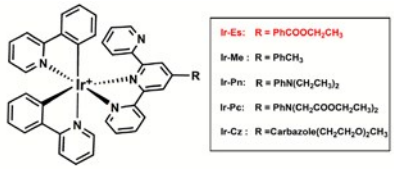

Scheme 1. The molecular structure of **Ir(III)** complexes.

In this work, we report terpyridine-based cyclometalated Iridium (III) complex that can be used as 2P-PDT agents and Iridium (III) is chosen as considering below. C-Ir metal bond, constructed by 2-phenyl pyridine, was used to stabilize the energy levels of the Ir complexes. Subsequently, the photophysical properties were tuned by using terpyridine derivatives, which used as bidentate ligand. Finally, terminal substitutes were modified to obtain different Ir(III) complexes to adjust their pull/push electronic capability and bio-affinity. Intriguingly, we found that complex **Ir-Es** could specifically target cell nucleus *via* intracellular microtubules dependent endocytosis and induced DNA binding. Subsequent two-photon irradiation triggered the immigration of **Ir-Es** from nucleus to mitochondria in living cells with efficient dual PDT damage, thus shedding light on the further practical utilization of **Ir-Es** as an anti-tumour agent. Compared with commercially available PS agent Chlorin e6 (*Ce6*, 660 nm),[12] **Ir-Es** displayed considerable inhibition (2P: 808 nm) towards solid tumour growth *in vivo* in a mouse model.

The detailed synthesis and characterization of Ir(III) complexes including **Ir-Es**, **Ir-Me**, **Ir-Pn**, **Ir-Pc** and **Ir-Cz** used in this study were stated in the Supporting information (Scheme S1, Fig. S1-S5). As expected, these complexes displayed singlet and triplet metal-to-ligand charge transfer (MLCT) ranging from 350 nm to 520 nm (Fig. S6 and Table S2),[13] and the emission bands were located in range of 570 - 600 nm (shift > 25 nm, Fig. S6). These

[a] School of Life Science, Anhui University, Hefei 230039, P. R. China
[b] Department of Chemistry, Key Laboratory of Functional Inorganic Material Chemistry of Anhui Province, Anhui University, Hefei 230039, P. R. China
[c] College of Pharmaceutical Sciences, Southwest University, Chongqing 400716, China
[d] Department of Chemistry, University College London, London WC1H 0AJ, UK
[e] Department of Chemical Engineering, University College London, London WC1H 0AJ, UK
[f] State Key Laboratory of Coordination Chemistry, Nanjing University, Nanjing 210093, P. R. China
* Correspondence: E-mail: xiaohe.t@ahu.edu.cn; yptian@ahu.edu.cn
‡ These authors contributed equally to this work.

View Article Online
DOI: 10.1039/C6CC

five complexes displayed varied luminescent lifetimes and quantum yields, indicating tunable emission properties of Ir (III) complexes.[14] The 2PA cross sections (σ) of the five Iridium complexes from 700-900 nm were shown in Fig. S7. The largest 2PA cross-sections of Ir complexes were located around 800 ± 30 nm with δ values between 60 - 110 GM.

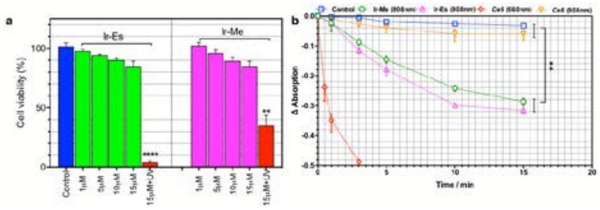

Fig. 1. *(a) HepG2 cells toxicity data under dark and UV light condition (24-hrs, interval=6 hours, 5 minutes/time) for* ***Ir-Es*** *and* ***Ir-Me*** *obtained from the MTT assay; (b) The decrease of absorption of ADPA (100 µM dissolved in PBS mixed with 5 µM* ***Ir-Es*** *and* ***Ir-Me****, respectively) with laser exposure for 0, 0.5, 1, 5, 10, 15 min.*

The impact of Iridium complexes treated cells under dark and irradiation condition was firstly evaluated by MTT assay. The cell viability of HepG2 (human liver cancer cell) (Fig. 1a and S8) as well as on non-cancerous HELF (human embryo liver fibroblast, Fig. S9) suggested that under dark incubation, **Ir-Es** displayed less invasive property (~85 %, 15 µM, 24 hours), whereas under UV irradiation a significant reduction in cell viability was detected. Compared with **Ir-Me** treated cells as showed in Fig. 1a, it is apparent that **Ir-Es** (~4% viability) possess more potency of phototoxic effects under UV condition than **Ir-Me** complex (~35% viability). This difference was interesting since the capability of singlet-oxygen generation form **Ir-Me** and **Ir-Es** showed no difference (Fig. 1b and Fig. S10), which indicated a chemical based method by monitoring the deduction of absorption of ADPA (9,10-Anthracenedipropionic acid),[5c] with Δ_{abs} = 0.2755 (**Ir-Es**, 15min) and 0.2875 (**Ir-Me**, 15min), respectively. Considering the significant oxygen consumption required by *Ce6*, moderate ROS generation nature of Ir(III) complexes might have more advantages particularly against hypoxic solid tumour, which bears by an inadequate oxygen supply.[15]

We therefore decided to evaluate the intracellular distribution of **Ir-Es**. The HepG2 cells were incubated with 5 µM complexes for 1 hour and MLCT (metal-to ligand charge transfer) emission and 2P confocal micrographs in living cells were successfully achieved (Fig. S11 and S12). It is notable that either from confocal images (Fig. 2a and 2b) or the single cell intensity profiles (Fig. S13), **Ir-Es** located in different subcellular compartment by contrast to the other Ir-complexes (**Ir-Me**, **Ir-Pn**, **Ir-Pc** and **Ir-Cz**). **Ir-Es** dominantly located in nuclear region, while other Ir(III) complexes distributed only in cytosolic space. The precise location in subcellular organelles was further confirmed by colocolization experiments using nuclear stains Hoechst 33342 (Hoechst) and mitochondrial marker Mitotracker Far-Red (MT-FR) (Fig. 2a and 2b). The confocal micrographs (and 3D micrographs, Fig. S14) strongly suggested that **Ir-Es** targeted intracellular nucleus (Pearson Correlation Coefficient Rr = 0.8384); in contrast, **Ir-Me** as a representative for the other four complexes, showed much less overlapping with nucleus but strong overlap with mitochondria (Fig. S15).

We speculated that the variation in cell uptake were due to different terminal moiety on **Ir-Es** and other Ir(III) complexes, consequently, leading to the disparate entry mechanism. Therefore, cell entry inhibition studies were performed (Fig. S16-S18) [16] and the intracellular intensity analysis suggested that **Ir-Es** cell entry could be considerably decreased by colchicine (microtubule-dependent endocytosis), a chemical could disrupt the polymerization of microtubules and further hinder endosomal trafficking; whereas the **Ir-Me** cell uptake was significantly reduced by several other inhibitors including choroquine (lysosomotropic agent), ammonia chioride (lysosomotropic agent) and chlorpromazine (clathrin-mediated endocytosis). As **Ir-Es** and **Ir-Me** shared the same backbone besides terminal substituent, we presumed that complexes' ester (**Ir-Es**) or methyl (**Ir-Me**) terminal might trigger specific microtubules dependent endocytosis or clathrin-mediated endocytosis, subsequently the former rerouted to cell nucleus and the latter accumulated within mitochondria, respectively. Their energy dependent cell entry pathways were further confirmed by incubating **Ir-Es** and **Ir-Me** with pre-fixed cells (Fig. S19). Compare to *in cellulo* results, both **Ir-Es** and **Ir-Me** showed a generalized cytosolic staining with no mitochondrial and nuclear specificity.

In addition to photoluminescence confocal microscopy, transmission electron microscopy (TEM) image of **Ir-Es** and **Ir-Me** complexes was used to confirm cellular distribution owing to the scattering electron capability of transition metal complex specifically accumulated at subcellular compartments.[17] HepG2 cells stained with osmium tetroxide (**OsO_4**) were used as control groups to show detailed information of intracellular membrane composition, such as nuclear membrane, vesicles and bilayer mitochondria structure (Fig. 2e, left). Compared to osmium tetroxide treated cells, Ir(III) complexes solely treated cells without **OsO_4** showed much weaker membrane contrast. However, **Ir-Es** treated cells presented reduced contrast in cytosolic regions, while significant greater contrast was detected in the nuclear space, suggesting that **Ir-Es** complex accumulated within cell nucleus (Fig. 2e, right). **Ir-Me** intracellular distribution (Fig. S20) displayed abundant cylinder-like structures in cytosol, which were highly correspondent to mitochondria. Considering the singlet-oxygen generation and living cell staining results obtained from **Ir-Es** complex, the PDT on HepG2 cells was carried out. **Ir-Me** did not present significant cell damage after initial (30-times, 800 nm) laser irradiation (Fig. S21). Its analogue **Ir(bpy)** (Figure S2 and S4 for characterization) also indicated relatively lower PDT efficiency with mitochondrial staining (Fig, S22 and S23). On the contrary, cells incubated with **Ir-Es** complex showed nuclear uptake and presented healthy morphology before light treatment (Fig. 3a). Once a smaller region was specifically selected (red line box) for laser irradiation (Fig. 3b), drastic morphology changes of cells could be clearly observed (Fig. 3c and 3d, black-dot box).

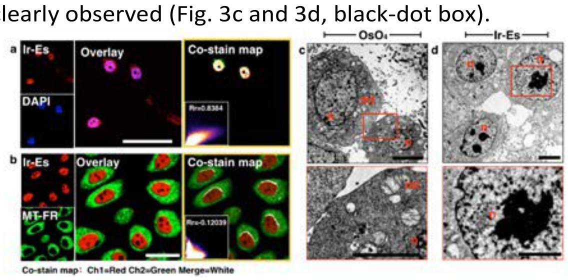

Fig. 2. *(a) and (b), HepG2 cells incubated with* ***Ir-Es*** *and co-localized with Hoechst 33342 and Mitotraker Far-Red (MT-FR), scale bar= 20 µm. (c) TEM microscopy of HepG2 cells stained with osmium tetroxide (d) solely incubated with* ***Ir-Es*** *without*

osmium tetroxide; Abbreviations: n = nucleus, mt = mitochondria. TEM scale bar= 5 µm.

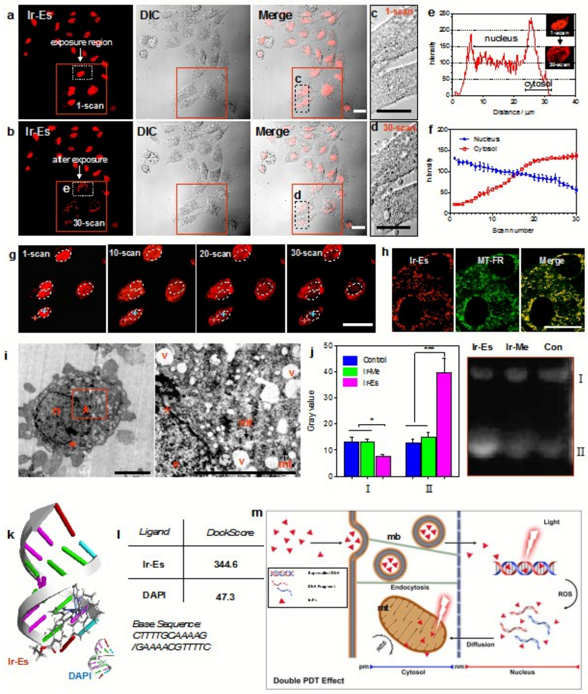

Fig. 3. *(a) 2P confocal micrograph before and (b) after continued irradiation at selected region (red box); (c) and (d) DIC micrographs showed the morphology before and after irradiation; (e) Single cell **Ir-Es** intensity profile before and after irradiation. (f) Cell intensity from nuclear and cytosolic region analysis over time after 30 scans. (g) Time series micrographs from selected region. (h) Colocolization **Ir-Es** complex and MT-FR after 2min continued 2P scanning. (i) TEM microscopy of HepG2 cells incubated with **Ir-Es** after UV light exposure. (j) Left: gray value intensity analysis showed Photocleavage effect of **Ir-Me** and **Ir-Es**. Right: Photocleavage of pBR322 DNA using **Ir-Me** and **Ir-Es** under illuminated condition. (k) Molecular docking between selected DNA segment and **Ir-Es** and DAPI with (l) docking scores. (m) Schematic representation of proposed **Ir-Es** complex intracellular PDT mechanism. Abbreviations: n=nucleus, mt=mitochondria, mb= microtubulin, pm=plasma membrane, nm=nuclear membrane. Scale bar = 10µm. $p < 0.005$. Error bars: SEM.*

It was noteworthy that during 30-time scanning, significant signals of **Ir-Es** immigrated from nuclear to cytosolic region and formed cylinder-like structure. The single cell intensity profile (Fig. 3e) clearly suggested that **Ir-Es** complex located in nuclear and cytosol before and after 800nm light treatment. Time-lapse micrographs (Fig. 3g, also refer to Fig. S movie-1 and S movie-2) indicated that **Ir-Es** complexes were gradually released from nuclear region and accumulated in cytosolic region upon laser irradiation (Fig. 3g), resulting in decreased fluorescence intensity of **Ir-Es** in nuclear and increased in cytosol, respectively (Fig. 3f). For comparison, the **Ir-Es** PDT effect under hypoxia condition was also performed with less cells damage and displayed no immigration (Fig. S24 and S25). The binding property of **Ir-Es** after the initial scans was confirmed by colocolization experiments with MT-FR under confocal microscopy and inductively coupled plasma mass spectrometry (ICP-MS) (Fig. S26). Due to the cationic nature of **Ir-Es**, high overlapping between **Ir-Es** complex and Mitotracker Far Red (Fig. 3h) was clearly observed, this also proved by ICP-MS evaluation. Additionally, the PDT impact on cell bioactivity after irradiation under **Ir-Es** and **Ir-Me** treatments were also quantitatively confirmed by mitochondria activity and nuclear permeability using classic JC-1[18] labelling kit and ANNEXIN-V FITC/PI (propidium iodide) double staining[19] kit, respectively. Both **Ir-Es** and **Ir-Me** treated cells showed significant mitochondrial damage after irradiation (Fig. S27) and emitted in green channel (λ_{Ex}=488 nm, λ_{Em}=500-520 nm). Whereas extensive FITC/PI double positive signals after continued two-photon treatment (800 nm, 180 s) demonstrated an effective PDT outcome (Fig. S28) that induced significant cell death and nucleus damage with permeable nuclear membrane; and relatively lower FITC and neglectable PI signal treated with **Ir-Me** under the same condition suggested why it was the localization difference matters. These results were further strengthened by TEM micrographs. The cells here were incubated with **Ir-Es** and received 4 illuminations within two hours incubation (illumination=30 s, interval=30 min), as comparison the **Ir-Me** group was also added (Fig. S29). In order to highlight the intracellular structure and membrane damage, we performed the second fixation using **OsO_4** for 1 hour. Compared to previous untreated cells under TEM (Fig. 2e, left), it clearly showed that after UV irradiation, **Ir-Es** treated cells contained abundant vacuoles, an organelle that plays a major role in early autophagy, leading to apoptotic cell death[20] (Fig. 3i, left). It had also clearly showed swollen mitochondria and misshapen nuclear structures in **Ir-Es** treated cells (Fig. 3i, right). In a good agreement with above confocal studies, the **Ir-Es** treated cells not only demonstrated considerable pre-autophagosomal structures (PAS) in cytosolic region, but also displayed much less contrast in nuclear region with a certain degree of nucleus misshapen or damage (red star). The above results highly suggested that an effective double damage had been occurred in **Ir-Es** treated cell sequentially from nucleus to mitochondria under irradiation, which was in a good agreement with the initial MTT assay that **Ir-Es** displayed a much stronger phototoxic response.

As **Ir-Es** located within nuclear in living cells, a model DNA was used to evaluate the capability of **Ir-Es** induced singlet-oxygen-mediated damage under light irradiation in cell-free experiments. The supercoiled pBR322 DNA treated with 30 µM **Ir-Es** and **Ir-Me** followed by 10 min illumination and 1 hour 37 ^{o}C incubation. Significant DNA cleavage was observed for **Ir-Es** treated group as the intensity of **Lane-I** (~2000 bp) was decreased and the intensity of **Lane-II** (~150 bp) was sharply increased (Fig. 3j). In contrast, at the same illuminated condition, **Ir-Me** complex with non-nuclear binding specificity showed much less DNA cleavage effect. The DNA cleavage effect of **Ir-Es** was confirmed *via* DNA binding experiments either in *in vitro* buffer solution (Fig. S30) and molecular modelling calculations using Discovery Studio Software (~9 fold stronger than DAPI, Fig. 3k and 3l, Fig. S31). [21]

Subsequently, on the basis of all of the results obtained above, we proposed a possible PDT mechanism (Fig. 3m): (1) **Ir-Es** with suitable positive charge, lipophilicity and ligand targeting moiety readily triggers microtubules dependent endocytosis across the plasma membrane and nuclear membrane, colocolized with DNA-riched chromatin or chromosomes. (2) Generated ROS induce DNA cleavage under two-photon irradiation and **Ir-Es** were released from nucleus, penetrated into cytosolic region. (3) **Ir-Es** binds to intracellular

mitochondria with high membrane potential ($\Delta\psi_m$),[22] induced secondary damage under continued 2P irradiation.

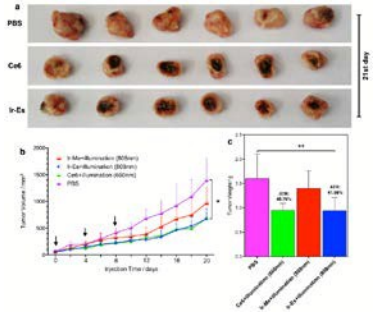

Fig.4 *(a) Solid tumour model treated with PBS, Ce6, and* ***Ir-Es****, the tumours were extracted at 21st day. (b) The growth curve and (c) growth inhibition rate of the solid tumour in the mice over 21 days under different treatment, the arrow indicated the injection (local) time point.*

To further assess the capability of Ir-Es as a potential PDT agent *in vivo,* mouse models were performed. The mice with solid tumour planted (n = 6) were treated with **Ir-Es** and **Ir-Me**, respectively. For comparison, *Ce6* a clinical PDT agent was applied, PBS and solely irradiation treated (660nm, 1400mA, Fig. 4 and Fig. S32) animals were also added as negative control. Fig. 4a directly presented the morphology of the tumour from mice after 21 days' treatment. As it measured daily in Fig. 4b, the volume of tumour treated with **Ir-Me** and under irradiation (808 nm, 600mA) is not significant difference from that treated with PBS. This suggested that although **Ir-Me** displayed certain damage towards cancerous cells *in vitro* in living cells, its *in vivo* PDT effect was very limited. On the contrary, when treated with **Ir-Es**, the growth of tumour was significantly inhibited (Fig. 4c, anti-tumour rate, ATR: 41.58 %) and similar to the outcome of the commercial PDT agents *Ce6* (ATR: 40.76 %). Predominated necrosis and apoptotic regions were also presented in Both H&E staining and Tunnel staining tumour tissue sections (Fig. S33) from groups treated **Ir-Es**.

In summary, we have designed and synthesized series of novel Iridium complexes and invested their photophysical properties in detail. With slightly modification on terminal substitute, these Iridium complexes were rerouted in nucleus (**Ir-Es**) and the mitochondria (**Ir-Me**, **Ir-Pn**, **Ir-Pc**, **Ir-Cz**), respectively. *In cellulo* studies revealed that **Ir-Es** complex presented low cytotoxicity in dark and displayed high cell damage under light irradiation. In particularly, we firstly demonstrated that a nuclear targeting complex **Ir-Es** generated significant 'double' damage sequentially form nucleus to mitochondria under two-photon irradiation, then successfully applied as a solid tumour growth inhibitor as a PDT agent using two-photon laser power. This study not only offers a competitive PDT candidate for therapeutic purpose, but also provides an idea on how to regulate the intracellular targeting within metallic molecular system *via* minor modification.

This work was supported by grants from the National Natural Science Foundation of China (21602003, 51432001, 51372003, and 51472002), Anhui Provincial Natural science foundation of China (1708085MC68), Anhui University Doctor Startup Fund (J01001962). We thank Dr. Martin R Gill (University of Oxford, Oxford, Department of Oncology) for useful suggestions and help discussions.

Notes and references

1 S. S. Lucky, K. C. Soo and Y. Zhang, *Chem. Rev.*, 2015, **115**, 1990-2042.
2 (a) M. Ethirajan, Y. H. Chen, P. Joshi and R. K. Pandey, *Chem. Soc. Rev.*, 2011, **40**, 340-362. (b)S. Wanninger, V. Lorenz, A. Subhan and F. T. Edelmann, *Chem. Soc. Rev.*, 2015, **44**, 4986-5002.
3 (a) G. Chen, I. Roy, C. Yang and P. N. Prasad, *Chem. Rev.*, 2016, **116**, 2826-2885. (b) J. P. Celli, B. Q. Spring, I. Rizvi, C. L. Evans, K. S. Samkoe, S. Verma, B. W. Pogue and T. Hasan, *Chem. Rev.,* 2010, **110**, 2795-2838.
4 M. C. DeRosa and R. J. Crutchley, *Coord. Chem. Rev*, 2002, **233**, 351-371.
5 (a) J. Ge, M. Lan, B. Zhou, W. Liu, L. Guo, H. Wang, Q. Jia, G. Niu, X. Huang and H. Zhou, *Nat. Comm*, 2014, **5**. (b) K. Liu, R. Xing, Q. Zou, G. Ma, H. Möhwald and X. Yan, *Angew. Chem. Int. Edit.*, 2016, **55**, 3036-3039. (c) S. Kim, T. Y. Ohulchanskyy, H. E. Pudavar, R. K. Pandey and P. N. Prasad, *J. Am. Chem. Soc.*, 2007, **129**, 2669-2675.
6 (a) H. Huang, B. Yu, P. Zhang, J. Huang, Y. Chen, G. Gasser, L. Ji and H. Chao, *Angew. Chem.*, 2015, **127**, 14255-14258. (b) W. Lv, Z. Zhang, K. Y. Zhang, H. Yang, S. Liu, A. Xu, S. Guo, Q. Zhao and W. Huang, *Angew. Chem.*, 2016, **128**, 10101-10105. (c) J. S. Nam, M. G. Kang, J. Kang, S. Y. Park, S. J. C. Lee, H. T. Kim, J. K. Seo, O. H. Kwon, M. H. Lim and H. W. Rhee, *J. Am. Chem. Soc.*, 2016, **138**, 10968-10977.
7 (a) A. Kachynski, A. Pliss, A. Kuzmin, T. Ohulchanskyy, A. Baev, J. Qu and P. Prasad, *Nat. Photonics*, 2014, **8**, 455-461.
8 (a) G. Bort, T. Gallavardin, D. Ogden and P. I. Dalko, *Angew. Chem. Int. Edit.*, 2013, **52**, 4526-4537. (b) M. Pawlicki, H. A. Collins, R. G. Denning and H. L. Anderson, *Angew. Chem. Int. Edit.*, 2009, **48**, 3244-3266. (c) B. K. Agrawalla, Y. Chandran, W. H. Phue, S. C. Lee, Y. M. Jeong, S. Y. Wan, N. Y. Kang and Y. T. Chang, *J. Am. Chem. Soc.*, 2015, **137**, 5355-5362.
9 K. K. W. Lo, *Account. Chem. Res.*, 2015, **48**, 2985-2995.
10 (a) A. Nakagawa, Y. Hisamatsu, S. Moromizato, M. Kohno, S. Aoki, *Inorg. Chem.*, 2013, **53**, 409-422. (b) S Moromizato, Y Hisamatsu, T Suzuki, Y. Matsuo, R. Abe, S. Aoki, *Inorg. Chem.*, 2012, **51**, 12697-12706. (c) A. Kando, Y. Hisamatsu, H. Ohwada, T. Itoh, S. Moromizato, M. Kohno, S. Aoki, *Inorg. Chem*., 2015, 54, 5342-5357.
11 (a) L. He, Y. Li, C. Tan, R. Ye, M. Chen, J. Cao, L. Ji and Z. Mao, *Chem. Sci*, 2015, **6**, 5409-5418. (b) Y. Yang, Q. Zhao, W. Feng and F. Li, *Chem. Rev.*, 2012, **113**, 192-270.
12 H. Dong, S. Du, X. Zheng, G. Lyu, L. Sun, L. Li, P. Zhang, C. Zhang and C. Yan, *Chem. Rev.*, 2015, **115**, 10725-10815.
13 (a) Y. Chen, L. Qiao, L. Ji and H. Chao, *Biomaterials*, 2014, **35**, 2-13. (b) S. Huo, J. C. Deaton, M. Rajeswaran and W. C. Lenhart, *Inorg. Chem.*, 2006, **45**, 3155-3157.
14 Q. Zhao, S. Liu, M. Shi, C. Wang, M. Yu, L. Li, F. Li, T. Yi and C. Huang, *Inorg. Chem.*, 2006, **45**, 6152-6160.
15 S. Thomas, M. A. Harding, S. C. Smith, J. B. Overdevest, M. D. Nitz, H. F. Frierson, S. A. Tomlins, G. Kristiansen and D. Theodorescu, *Cancer Res.*, 2012, **72**, 5600-5612.
16 (a) H. K. Ziegler and E. R. Unanue, *Proc. Nat. Acad. Sci. USA* 1982, **79**, 175-178. (b) C. A. Puckett and J. K. Barton, *Biochem.*, 2008, **47**, 11711-11716.
17 M. R. Gill, J. Garcia-Lara, S. J. Foster, C. Smythe, G. Battaglia and J. A. Thomas, *Nat. Chem*, 2009, **1**, 662-667.
18 A. Cossarizza, M. Baccarani-Contri, G. Kalashnikova and C. Franceschi, *Biochem. Biophys. Res. Commun.*, 1993, **197**, 40-45.
19 A. P. Thomas, P. S. Saneesh Babu, S. Asha Nair, S. Ramakrishnan, D. Ramaiah, T. K. Chandrashekar, A. Srinivasan and M. Radhakrishna Pillai, *J. Med. Chem.*, 2012, **55**, 5110-5120.
20 N. Mizushima, *Gene. Dev.*, 2007, **21**, 2861-2873.
21 G. Wu, D. H. Robertson, C. L. Brooks and M. Vieth, *J. Comput. Chem.*, 2003, **24**, 1549-1562.
22 Y. Chen, L. Qiao, L. Ji and H. Chao, *Biomaterials*, 2014, **35**, 2-13.